The Permeability of the Nuclear Envelope in Dividing and Nondividing Cell Cultures

Carl M. Feldherr and Debra Akin

Department of Anatomy and Cell Biology, University of Florida, Gainesville, Florida 32610

Abstract. The objective of this study was to determine whether the permeability characteristics of the nuclear envelope vary during different phases of cellular activity. Both passive diffusion and signal-mediated transport across the envelope were analyzed during the HeLa cell cycle, and also in dividing, confluent (growth-arrested), and differentiated 3T3-L1 cultures. Colloidal gold stabilized with BSA was used to study diffusion, whereas transport was investigated using gold particles coated with nucleoplasmin, a karyophilic *Xenopus* oocyte protein. The gold tracers were microinjected into the cytoplasm, and subsequently localized within the cells by electron microscopy. The rates of diffusion in HeLa cells were greatest during the first and fifth hours after the onset of anaphase. These results correlate directly with the known rates of pore formation, suggesting that pores are more permeable during or just after reformation. Signal-mediated transport in HeLa cells occurs through channels that are located within the pore complexes and have functional diameters up to 230–250 Å. Unlike diffusion, no significant differences in transport were observed during different phases of the cell cycle. A comparison of dividing and confluent 3T3-L1 cultures revealed highly significant differences in the transport of nucleoplasmin-gold across the envelope. The nuclei of dividing cells not only incorporated larger particles (230 Å versus 190 Å in diameter, including the protein coat), but the relative uptake of the tracer was about seven times greater than that in growth-arrested cells. Differentiation of confluent cells to adipocytes was accompanied by an increase in the maximum diameter of the transport channel to ~230 Å.

THERE are potentially two general mechanisms for controlling macromolecular exchanges between the nucleus and cytoplasm. The first is dependent on the physical and chemical properties of the permeant molecules. Modulation of these properties can affect both passive diffusion and transport across the nuclear envelope. Diffusion occurs through aqueous channels, ~100 Å in diameter, that are located in the centers of the nuclear pore complexes. The rates of exchange are inversely related to molecular size, and substances larger than ~70 kD are effectively excluded from the diffusion channel (22, 23). Molecules or molecular aggregates as large as 260 Å in diameter can be actively transported across the pores if they contain appropriate nuclear targeting sequences (4, 8). However, the rates of transport, as well as the size of the transport channel, are variable, and known to be dependent on both the number and the specific amino acid composition of the targeting signals (2, 4).

A second possible regulatory mechanism could involve modifications of the permeability characteristics of the pore complexes, caused by changes in cellular activity. Although this concept has important functional implications, very little pertinent data is available. Jiang and Schindler (14) reported changes in the nuclear uptake of fluorescein-labeled dextrans in 3T3 cells after treatment with epidermal growth factor and insulin. Feldherr (6, 7) investigated the intracellular distribution of polyvinylpyrrolidone (PVP)[1]-coated gold particles in dividing amebas, and observed that the nuclei were most permeable during the first 2 h after division. Since neither dextran nor PVP contain nuclear targeting signals, these results reflect changes in passive diffusion across the envelope. Currently, there is no information regarding modifications in signal-mediated nuclear transport.

The purpose of this study was to determine whether the properties of the nuclear pore complexes vary during different periods of activity in specific cell types. Both diffusion and transport of macromolecules across the envelope were analyzed throughout the HeLa cell cycle, and also in dividing, confluent (growth-arrested) and differentiated 3T3-L1 cells. Colloidal gold particles coated with BSA were used to study passive diffusion. Gold coated with either nucleoplasmin or BSA conjugated with peptides containing the SV40 nuclear targeting signal was used in transport studies. The colloidal tracers were microinjected into the cytoplasm, and their subsequent intracellular distribution was determined by electron microscopy. Using this experimental approach, relative nuclear uptake, as well as the dimensions of the exchange channels, could be analyzed.

1. *Abbreviations used in this paper*: N/C, nuclear to cytoplasmic; PVP, polyvinylpyrrolidone.

Significant variations in passive diffusion across the envelope were detected at different times in the HeLa cell cycle. A close correlation exists between the peaks of diffusion and the maximum rates of nuclear pore formation. In addition, significant differences in both the relative nuclear uptake of nucleoplasmin-gold and the dimensions of the transport channel were detected during different functional states in 3T3-L1 cells.

Materials and Methods

Culture and Synchronization Procedures

HeLa cells were maintained in T25 flasks in 5% CO_2 at 37°C and subcultured every 3 d. The culture fluid consisted of Minimum Essential Media (Alpha-Mem) containing 10% FBS, penicillin G (10,000 U/ml), streptomycin sulfate (10 mg/ml), and fungizone (250 μg/ml). All tissue culture reagents were purchased from Gibco Laboratories (Grand Island, NY).

Before microinjection of HeLa cells, mitotic shake-offs were performed as follows: cell aggregates and debris were removed from 1- to 2-d-old cultures by slowly pouring off the culture medium; fresh medium was added, and the flasks were gently shaken. The dissociated cells were then plated on gridded, collagen-coated ACLAR cover slips (see below) that were attached to the bottom of 35-mm Petri dishes. 60% of the cells that were obtained by this procedure were in metaphase, anaphase, or telophase; 30% were in early interphase, as judged from their size; the remaining 10% could not be characterized. These cultures were used to study nuclear permeability at the later stages of the cell cycle (7–20 h). At earlier periods in the cycle (15 min to 5 h), greater precision was required and it was necessary to time the cells individually. To accomplish this, the shake-off cultures were grown in an incubator for ~20 h, at which time they were transferred to an inverted Nikon microscope fitted with an environmental chamber that was maintained at 37°C. Carbon dioxide was supplied to keep the pH of the cultures at 7.4, and mineral oil was added to the surface of the medium to prevent evaporation. Cells just entering anaphase (0 time) were identified, their position on the ACLAR cover slip was recorded and they were injected 15 min to 5 h later. The time required for progression of the cells through mitosis was the same as described by Robbins and Gonatus (25).

3T3-L1 cells were grown in DME supplemented with FBS, penicillin G, streptomycin, and fungizone (at concentrations given above), and kept at 37°C in 5% CO_2. Subculturing was carried out as described by Frost and Lane (10); the cells were discarded after the tenth passage. Dividing, confluent, and differentiated cells to be used for nuclear permeability studies were prepared as follows: dividing populations were obtained from mitotic shake-offs of nonconfluent stock cultures. The cells were transferred to ACLAR cover slips in 35-mm Petri dishes (see below) and incubated for 8 h before microinjection. Confluent cultures were prepared by inoculating ACLAR Petri dishes with trypsinized cells at a density of 2.0×10^5 cells/ml; confluency was reached in 4–6 d. Differentiation of the confluent cells into adipocytes was accomplished by the addition of methylisobutylxanthine, dexamethasone, and insulin to the cultures (10).

ACLAR (a fluoroplastic obtained from Allied Chemical) proved to be an excellent substrate for culturing and processing cells for electron microscopy (15). Before culturing, a grid pattern with ~1-mm spacing was scored on the surface of the ACLAR (18). This provided a convenient means of mapping injected and dividing cells; furthermore, since the pattern was etched on the surface of the plastic blocks after embedding, individual cells could be readily identified for electron microscopic analysis. To facilitate attachment of HeLa cells, the ACLAR was coated with collagen as described by the supplier (Sigma Chemical Co., St. Louis, MO). Pretreatment was not required for 3T3-L1 cells.

Gold Preparation and Microinjection

Colloidal gold fractions containing particles 20–120 Å in diameter were prepared by reducing gold chloride with a saturated solution of phosphorus in ether (5). Larger particles, ranging in diameter from 80 to 240 Å and above, were obtained by using sodium citrate as a reducing agent (9). The size of the fractions varied slightly in different preparations. The gold particles were coated with BSA (Sigma Chemical Co.), nucleoplasmin, or BSA conjugated with synthetic peptides containing either active (WT) or inactive (cT) SV40 nuclear targeting signals. Nucleoplasmin was isolated from *Xenopus* oocytes by antibody affinity chromatography (4), and the BSA conjugates were prepared and analyzed as described in detail by Lanford et al. (16). Both the BSA-WT and BSA-cT conjugates contained an average of eight signal sequences per BSA molecule. Before injection all stabilized gold fractions were dialyzed against intracellular medium that consists of 117 mM KCl, 10.1 mM NaCl, 6 mM K_2HPO_4, and 4 mM KH_2PO_4 (pH 7.0). Unless otherwise indicated, the dimensions of the gold particles given in this report do not include the protein coat, which increases the overall particle diameter by ~30 Å.

Microinjection was performed using an inverted microscope (Nikon Diaphot) and a Narishige hydraulic micromanipulator. The microscope was enclosed in an environmental chamber that was kept at 37°C; CO_2 was provided to maintain the pH of the cultures at 7.4. The micropipets had outside tip diameters of ~0.5–0.7 μm. A continuous flow injection system was used (11).

Electron Microscope Procedures

The experimental cells, still attached to ACLAR, were fixed by adding an equal volume of 2% glutaraldehyde in 0.2 M cacodylate buffer (pH 7.3) directly to the cultures. After 30 min to 1 h at room temperature, or overnight at 4°C, the cells were rinsed in buffer, and postfixed in a mixture of 1% OsO_4 and 1% $K_4Fe(CN)_6$ in 0.1 M cacodylate buffer (pH 7.3) for 1 h at room temperature. The cells were then rinsed in deionized H_2O, dehydrated through a graded ethanol series followed by acetone, and embedded in Spurr's low viscosity resin (26). After curing, the ACLAR was removed from the resin leaving behind the cells and an impression of the grid pattern.

The cells of interest were cut out of the block, remounted, and sectioned using an MT-2 microtome fitted (Sorvall, Inc., Norwalk, CT) with a diamond knife. The sections were picked up on formvar-coated slot grids and examined using a JEOL 100CX electron microscope. To facilitate detection of the gold particles, the sections were not poststained.

Results

Diffusion across the Nuclear Envelope in HeLa Cells

BSA-coated gold particles, 20–120 Å in diameter, were microinjected into the cytoplasm of HeLa cells at various times after division. The cells were fixed 30 min later, and relative nuclear uptake was determined by counting particles in equal, randomly selected areas of nucleoplasm and cytoplasm in electron micrographs. A typical micrograph of an injected cell is shown in Fig. 1.

The nuclear uptake data, expressed as nuclear to cytoplasmic (N/C) ratios, are given in Fig. 2. Maximum influx of BSA-gold into the nucleoplasm occurred 15–45 min after the beginning of anaphase. This was followed by a statistically significant decrease at 1–2 h ($P < 0.05$), a further decrease at 2–3 h ($P < 0.05$), and a significant increase at 4–5 h ($P < 0.05$). The subsequent decreases at 7 and 19 h were significantly less than the values obtained for the 4–5-h individually timed cells, but not the 4–5-h mitotic shake-offs.

Table I compares the size distribution of BSA-gold particles present in the cytoplasm (i.e., particles available for diffusion), and nucleoplasm of cells injected 15–45 min, 1–2 h, and 4–5 h after division. These data were obtained by measuring all particles in randomly selected areas within the two compartments. The regions of nucleoplasm and cytoplasm analyzed were not equivalent. The results indicate that the exclusion limit for diffusion is ~120–130 Å (including the 30-Å protein coat) at each of the times analyzed. A comparison of the size distribution of the gold tracer at other time intervals was not attempted due to the limited number of particles present in the nucleoplasm.

To determine if the rapid diffusion of tracer into the nucleoplasm of cells injected 15–45 min after division was

Figure 1. An electron micrograph of a HeLa cell that was injected with BSA-gold 2.5 h after mitosis and fixed 30 min later. Gold particles are distributed throughout the cytoplasm (*C*), but, at this time in the cell cycle, they are essentially excluded from the nucleus (*N*). Bar, 0.5 μm.

due to incomplete reformation of the nuclear envelope at the time of injection, five cells were fixed 6–24 min after the start of anaphase and examined with the electron microscope. Even at these early times the envelopes appeared intact and seemed to form continuous boundaries around the daughter nuclei. The observation that the upper size limit for diffusion is the same at 15–45 min (~120–130 Å) as it is at later times provides additional evidence for the integrity of the envelope. Further confirmation that the exclusion limit is not greater at early time points was obtained by injecting 80–240 Å BSA-coated particles into 8–40 min postmetaphase cells. 12 cells were injected, and, in all instances, gold was found only in the cytoplasm.

Since changes in the size of the nucleus can affect diffusion rates (see Discussion), nuclear volumes were analyzed 20 min and 2 h after the start of division in individually timed cells. The dimensions of the ellipsoid nuclei were obtained as follows: the length and width were measured from face views in whole plastic embedded cells. Thin (0.5-μm) perpendicular sections were then cut and used to determine nuclear thickness. The calculated volumes at 20 min and 2 h (258 and 263 μm^3, respectively) were not significantly different.

Nuclear Transport in HeLa Cells

Signal-dependent transport across the nuclear envelope was studied by microinjecting gold particles (80–240 Å in di-

Table I. Size Distribution of BSA-gold in HeLa Cells

Time	No. of particles measured	Percentage of particles in each size class*				
		20–40 A	40–60 A	60–80 A	80–100 A	100 A+
15–45 min	CYTO 1597	10.8	48.8	29.2	9.7	1.4
	NUC 987	15.9	54.7	24.0	4.6	0.7
1–2 h	CYTO 483	15.5	43.1	31.3	7.2	2.9
	NUC 241	23.6	46.9	23.6	5.4	0.4
4–5 h	CYTO 453	9.9	39.9	30.2	17.4	2.4
	NUC 232	19.8	49.1	28.0	2.4	0.4

* Dimensions do not include the thickness of the coat material.

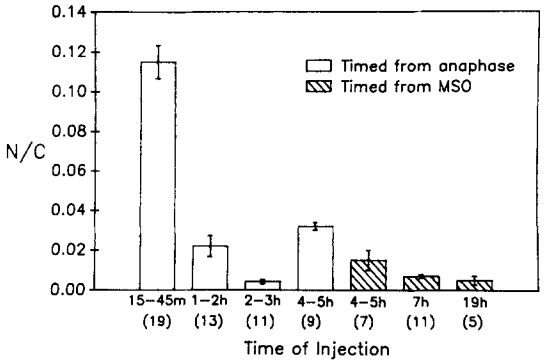

Figure 2. Relative nuclear uptake of BSA-gold at different times in the cell cycle was determined by counting particles in equal and adjacent areas of nucleoplasm and cytoplasm. Uptake is expressed as N/C ratios; standard errors are indicated. The number of cells examined at each time interval is given in parentheses. The total number of particles (nucleus plus cytoplasm) counted at the different times were 13,796 at 15–45 min; 10,042 at 1–2 h; 9,006 at 2–3 h; 10,252 at 4–5 h (timed from anaphase); 1,897 at 4–5 h (*MSO*); 4,906 at 7 h; and 728 at 19 h.

ameter) coated with nucleoplasmin or BSA-WT conjugates into the cytoplasm at various times in the cell cycle. The cells were fixed for electron microscopy 15 min after injection, and relative nuclear uptake was measured as described above. In preliminary experiments, it was determined that increasing the interval between injection and fixation from 15 min to as long as 7 h did not significantly increase the N/C ratio.

The intracellular localization of nucleoplasmin-gold is illustrated in Fig. 3. The cell shown in this electron micrograph was injected 8.5 h after division; however, the same gold distributions were observed after 25–30 min, 4.5 h, and 17–20 h. Within the cytoplasm, localized concentrations of gold particles were seen along the surfaces of pores that were present in structures resembling elements of the endoplasmic reticulum. Cytoplasmic pores have been described previously (19), but their origin and function is not known. Accumulations of nucleoplasmin-coated particles were also observed just adjacent to and within the centers of the nuclear pore complexes. Gold was routinely found, in high concentrations, within the nucleoplasm, but was excluded from the nucleoli.

Fig. 4 shows the N/C ratios obtained for transported particles at various periods in the cell cycle. Relative nuclear uptake was not significantly different at any of the time periods examined, as determined by *t*-test analysis. Particles coated with BSA-WT conjugates were also transported but in significantly lower amounts than nucleoplasmin-gold ($P < 0.01$ at both 4.5 and 8.5 h). Gold stabilized with BSA-cT conjugates, which contain inactive SV40 signals, was excluded from the nucleus.

Size measurements revealed that nucleoplasmin-coated particles with diameters of at least 160–200 Å readily en-

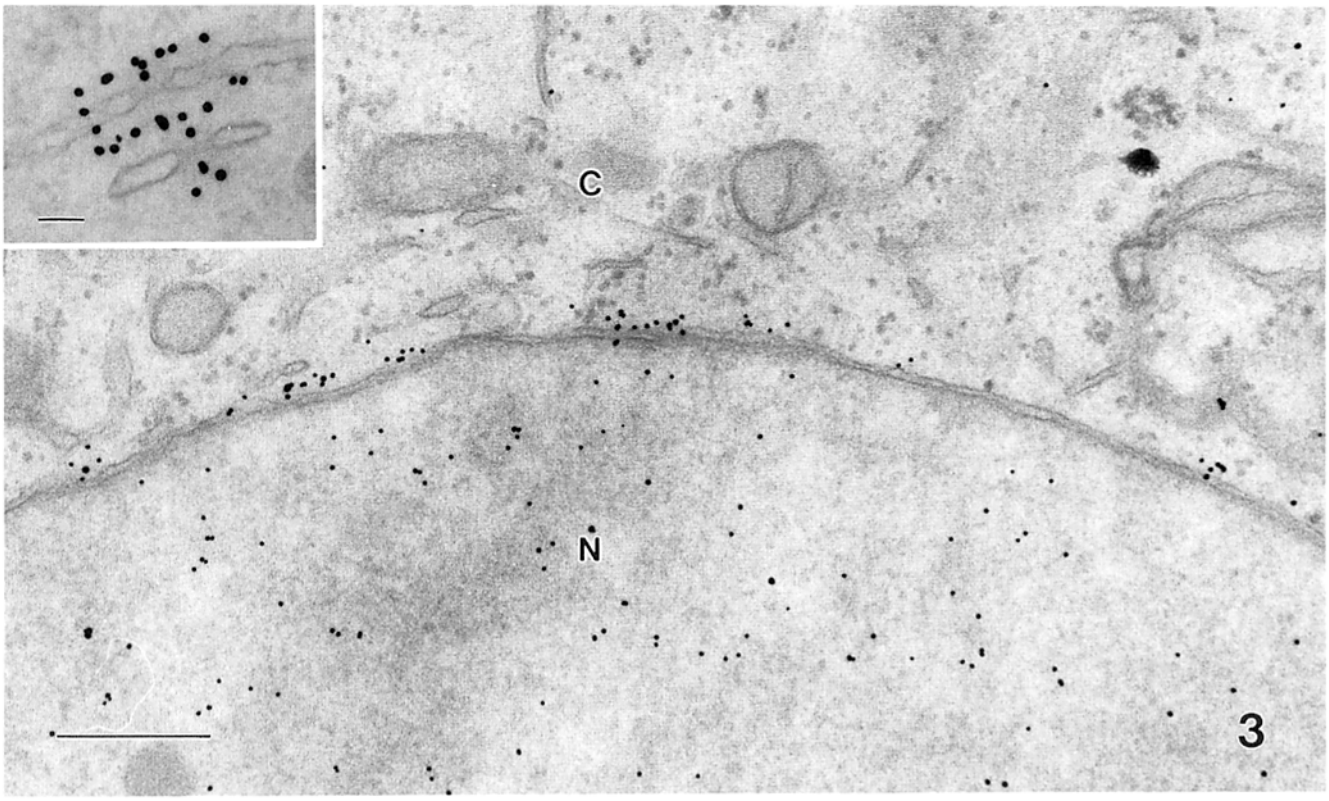

Figure 3. An electron micrograph of a 8.5-h-old HeLa cell injected with nucleoplasmin-gold particles and fixed after 15 min. By this time gold had accumulated within the nucleus (*N*). Transport of particles at large as 250 Å in diameter (including the coat material) occurred through channels located within the pore complexes. The inset shows the association of gold particles with cytoplasmic pores. *C*, cytoplasm. Bar, 0.5 μm; inset bar, 0.1 μm.

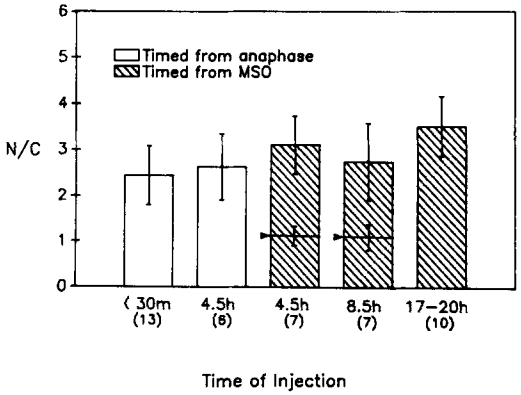

Figure 4. The N/C ratios of nucleoplasmin-gold that was injected into HeLa cells at different times in the cell cycle. Standard errors are shown. The number of injected cells is given in parentheses. 1,210 nucleoplasmin-coated particles were counted at 25–30 min; 2,500 at 4.5 h (timed from anaphase); 1,211 at 4.5 h (*MSO*); 1,972 at 8.5 h; and 629 at 17–20 h. The values indicated by arrowheads at the 4.5- and 8.5-h time points represent the ratios obtained for BSA-WT conjugates. 10 and 18 cells were injected with BSA-WT-coated gold at 4.5 and 8.5 h, respectively.

tered the nucleus at all time intervals. The combined data comparing the dimensions of the particles in the cytoplasm and nucleoplasm are given in Fig. 5. It is estimated, after correcting for the protein coat, that the maximum diameter of the transport channel in HeLa cells is ~230–250 Å.

Nucleocytoplasmic Exchange in 3T3-L1 Cells

Cells in dividing and confluent (growth-arrested) 3T3-L1 cultures (Fig. 6, *a* and *b*) were microinjected with either 20–120 Å particles coated with BSA or 80–240 Å fractions stabilized with nucleoplasmin, and fixed after 30 min. BSA-gold was restricted to the cytoplasm of all injected cells, while nucleoplasmin-coated particles were present within the nuclei in both experimental groups. Nucleoplasmin-gold was associated with cytoplasmic and nuclear pores, but was excluded from the nucleoli. Fig. 7 is an electron micrograph illustrating the gold distribution in a cell from a dividing population. Although nuclear transport occurred during both

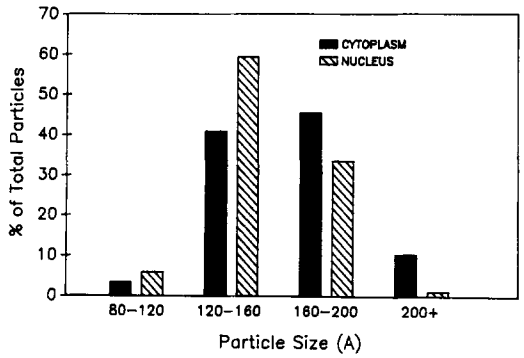

Figure 5. The size distributions of nucleoplasmin-coated gold particles present in the nucleus and cytoplasm of injected HeLa cells. These distributions represent the combined data of all time points examined. 690 nuclear and 673 cytoplasmic particles were measured.

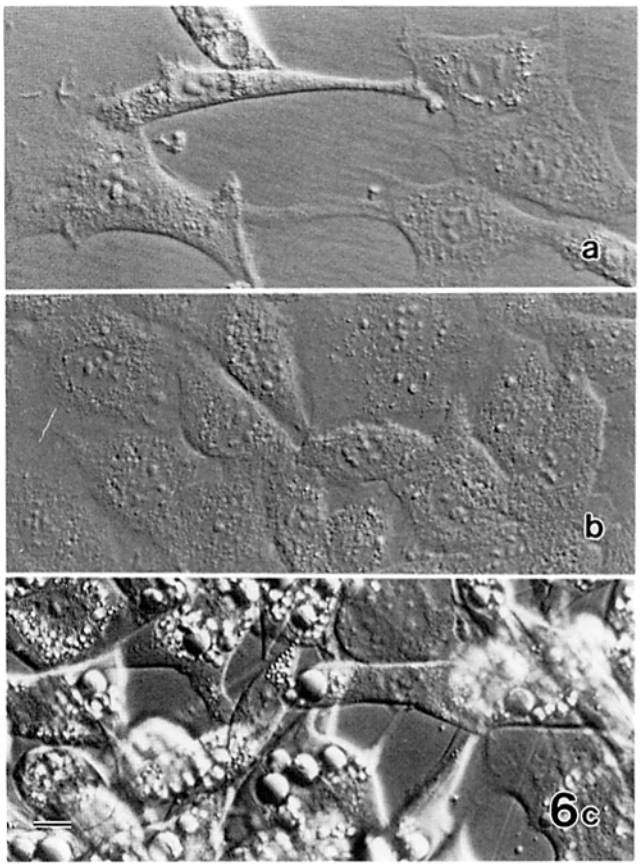

Figure 6. Modulated contrast images of typical experimental cells in dividing (*a*), confluent (*b*), and differentiated (*c*) 3T3-L1 cultures. Bar, 10 μm.

functional states (see Table II), the N/C ratio was significantly greater in dividing cells ($P << 0.01$).

The size distributions of the nucleoplasmin-coated gold particles in the nuclei of dividing and confluent cells are shown in Fig. 8. The dimensions of the cytoplasmic particles are included for comparison. In dividing populations, particles at least 200 Å in diameter were transported across the nuclear envelope, whereas the upper limit for transport in confluent cells was ~160 Å. The difference in the dimensions of the nuclear particles is highly significant ($P << 0.01$), as determined by chi-square analysis. To establish whether these results were due to restricted migration of the larger particles within the cytoplasm of the confluent cells, the size distribution of the gold immediately adjacent to the nuclear envelope was compared in the two experimental groups. No differences were detected, demonstrating that the particles were equally accessible to the nucleus.

11 adipocytes (Fig. 6 *c*) were injected with nucleoplasmin-coated particles that ranged from 80 to 300 Å in diameter. Due to the difference in fraction size, the N/C gold ratio (0.18), obtained for adipocytes, cannot be compared directly to the ratios determined for growing and confluent cells. However, the larger fraction was especially useful for establishing the exclusion limit for nuclear transport. In this regard, it can be seen in Fig. 9 that the maximum size particles present in adipocyte nuclei were ~200 Å in diameter, indicating that differentiation of the confluent cells is accompa-

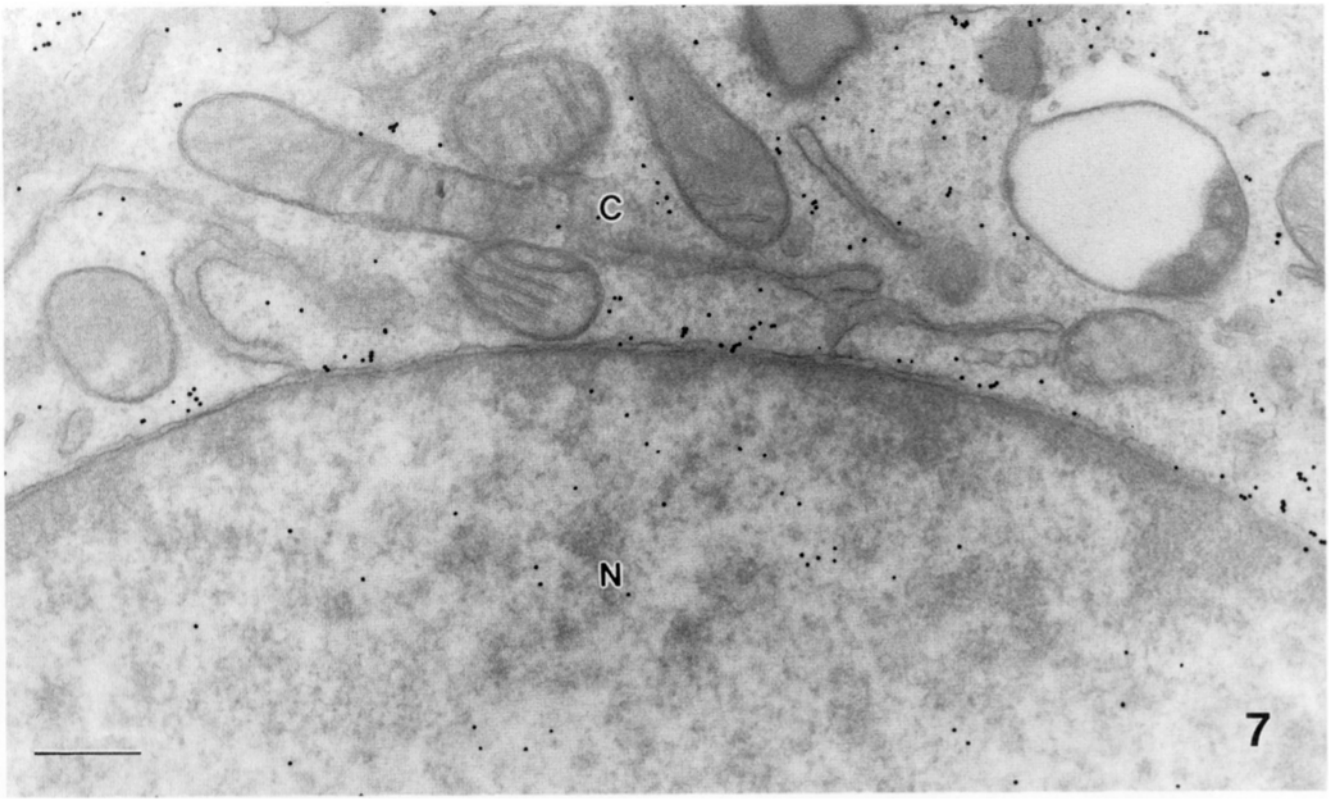

Figure 7. 30 min after injecting nucleoplasmin-gold into cells in dividing 3T3-L1 cultures, particles could be seen distributed throughout the nucleus (*N*) and cytoplasm (*C*), and were also associated with the nuclear pores. Bar, 0.5 μm.

nied by a change in the functional properties of the nuclear pore complexes.

The mean diameters ± SE of the nuclear pores (the circular apertures formed by membrane fusion) in dividing, confluent, and differentiated cells were found to be 728 ± 5.8; 698 ± 4.3; and 721 ± 5.0 Å, respectively (n = 200 in each group). Statistical analysis of the data showed that the size of the pores in confluent cells is significantly less than that in either dividing or differentiated populations ($P < 0.01$ and < 0.02, respectively). All pore measurements were made at 20,000× from sections cut perpendicular to the nuclear envelope. Only those pores in which the membrane boundaries could be clearly delineated were analyzed.

Discussion

The pattern obtained for the nuclear incorporation of BSA-gold demonstrates that, in HeLa cells, peak periods of diffusion across the nuclear envelope occur during the first and fifth hours after the onset of anaphase. Since reassembly of the envelope is completed within 15 min after division (see Results and also reference 25), the uptake data, even at the earliest experimental time points, manifests the permeability properties of the nuclear pore complexes, and cannot be accounted for by the direct exchange of gold through breaks in the membranes of the envelope.

Variations in the surface area to volume ratio, or more specifically, the nuclear pore to volume ratio, could significantly affect the uptake of diffusible molecules into the nucleus. However, the available data suggest that this factor could not explain the BSA-gold results. For example, no significant

Table II. Nuclear Transport in 3T3-L1 Cells

Functional state of cells	No. of cells examined	Total particle count	N/C ± SE
Dividing	14	2,688	0.67 ± 0.059
Confluent	31	3,241	0.09 ± 0.0015

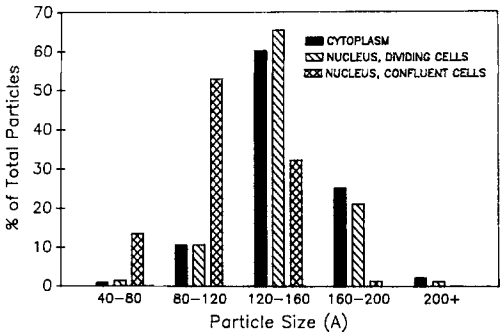

Figure 8. A comparison of the size distributions of nucleoplasmin-gold particles that entered the nuclei of dividing and confluent 3T3-L1 cells within 30 min after injection (577 and 690 particles were measured, respectively). The cytoplasmic data show the dimensions of the particles that were available for transport in both experimental groups. 1,755 cytoplasmic particles were measured.

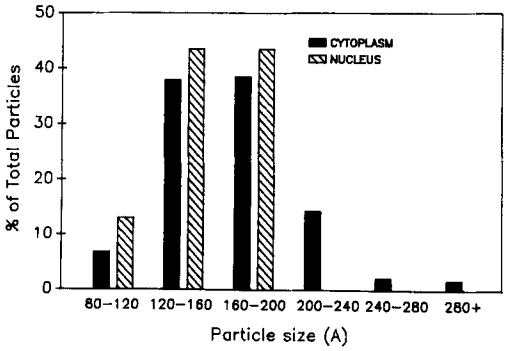

Figure 9. The size distributions of nucleoplasmin-coated gold particles located in the nucleus and cytoplasm of adipocytes 30 min after injection (115 and 893 particles were measured, respectively).

change in nuclear volume was found to occur between 20 min and 2 h postmetaphase, although the number of pores is known to increase during this period (20). The resulting increase in the pore to volume ratio would favor an increase in diffusion during the second hour after division; instead, however, a significant decrease was observed. Subsequent fluctuations in diffusion rates also fail to correlate with predicted pore to volume ratios.

The most likely explanation for the BSA-gold diffusion pattern is based on results reported by Maul et al. (20). These investigators found that although the number of nuclear pore complexes in HeLa cells increases throughout the cell cycle, the rate of pore formation is not uniform. The rate is greatest 0–1 h after division (25 pores/min), it decreases to ~1.5 pores/min at 2–3 h and reaches a second peak at 4–5 h (4–6 pores/min). This is followed by a continuous decrease in the formation rate throughout the remainder of the cell cycle. These data correlate very closely with BSA-gold uptake.

The direct relationship between the rates of diffusion and pore production suggests that newly forming pores comprise a subpopulation that is more permeable than fully reconstituted, mature pore complexes, and that BSA-gold influx is dependent on the size of this subpopulation. The observation that the exclusion size for BSA-gold was the same at all time intervals examined, regardless of the nuclear uptake rates, argues against the alternative explanation that variations in diffusion are due to changes in the functional size of the available exchange sites.

At present, there is no data available regarding either the molecular mechanism of pore assembly or the time required for pore complex maturation. The physiological significance of the uptake peaks is also unclear, although the rapid rate of diffusion immediately after division could facilitate nuclear reformation.

Increased diffusion of gold particles across the nuclear envelope was also reported after division of the amebas *Chaos chaos* (6) and *Amoeba proteus* (7), but it is not known whether uptake in these cells is related to pore formation. Swanson and McNeil (27) studied the nuclear incorporation of fluorescein-labeled dextrans during division in fibroblasts and failed to detect an increase in diffusion; however, differences in the experimental procedures make it difficult to compare their results with those obtained using colloidal gold.

Gold particles, 80–240 Å in diameter, that are too large to diffuse across the envelope, readily enter the nuclei of HeLa cells if they are coated with nucleoplasmin or BSA-conjugates that contain active nuclear targeting signals. The relative nuclear uptake (N/C ratio) of transported particles remained constant throughout the cell cycle. Thus, changes in metabolic activity that occur during the cycle do not appear to be accompanied by variations in nuclear transport.

In general, the intracellular distribution of the targeted particles in HeLa cells was similar to that reported for *Xenopus* oocytes (4, 8). Nucleoplasmin-gold was localized within and adjacent to the nuclear pore complexes (also see references 21 and 24), supporting the view that these structures are the primary sites for nucleocytoplasmic exchange. Based on the size of the gold particles present in the nucleoplasm, the transport channel in HeLa cells is estimated to be ~230–250 Å in diameter. In addition, tracer particles were associated with cytoplasmic pores, indicating that they also contain receptors for nuclear targeting sequences. The effectiveness of the transport process at the early time points (25–30 min) is consistent with the results reported by Benavente et al. (3), who found that the pores became functional as early as telophase.

Although no modifications in nuclear transport were observed during the HeLa cell cycle, statistically significant changes occurred during different functional states in 3T3-L1 cells. Reduction in overall metabolic activity that occurs during confluency (17) was accompanied by decreases in both relative nuclear uptake and the dimensions of the transport channel. The permeability changes appear to be reversible, as indicated by the fact that differentiation to adipocytes was associated with an increase in channel size. These results demonstrate that in addition to variations in the size and signal content of the permeant molecule, nuclear transport can be controlled by alterations in the properties of the pores themselves. Such changes have obvious regulatory implications, especially since shifts in the exclusion limit occur within a size range that could significantly affect the efflux of RNP particles from the nucleus. Whether the permeability modifications are limited to rate and size effects, or whether the specificity of the transport receptors also changes, has yet to be determined.

Jiang and Schindler (14) investigated the nuclear uptake of fluorescein-labeled dextrans in 3T3 fibroblasts, and reported that epidermal growth factor and insulin increased nuclear uptake in adhering, but not spherical cells. These data imply that modulation of cellular activity is accompanied by changes in nuclear permeability and, furthermore, suggest that the process is related to cell shape. However, since dextran was employed as a tracer, the results pertain only to changes in diffusion across the envelope. It cannot be assumed that mediated transport is similarly affected.

There are three likely explanations for the fluctuations in transport that were observed in 3T3-L1 cells. First, the composition of the pore complex could vary. Modifications in any one of a number of components, such as receptors, structural elements or transducing factors could influence transport rates and channel size. Second, changes in transport could result from alterations in overall pore diameter. According to this proposal, the composition and organization of the eight pore complex subunits would remain essentially unchanged; however, the distance between the inner margins of the subunits and the pore centers would vary as a function

of pore size. Since the margins of the subunits (or associated structures [1]) appear to form the boundaries of the diffusion and transport channels, one would expect corresponding changes in both the exclusion limits and rates of nucleocytoplasmic exchanges. Differences in pore diameter, which, in fact, were detected in this investigation, could result from alterations in nuclear shape that are known to accompany changes in cell function (12, 13). These shape changes most likely reflect reorganization of elements of the cytoskeletal and nuclear matrix. Third, fluctuations in transport could be due to changes in overall energy levels during different functional states. In future experiments it should be possible to distinguish among these alternatives.

The authors are grateful to Dr. Robert Lanford for supplying the BSA-WT and cT conjugates, to Dr. Robert Cohen for critically reviewing the paper, and to Dr. Ailene Feldherr for her assistance in preparing the manuscript.

This work was supported by National Science Foundation grant DCB-8711330.

Received for publication 26 January 1990 and in revised form 12 March 1990.

References

1. Akey, C. W. 1989. Interactions and structure of the nuclear pore complex revealed by cryo-electron microscopy. *J. Cell Biol.* 109:955–970.
2. Akey, C. W., and D. S. Goldfarb. 1989. Protein import through the nuclear pore complex is a multistep process. *J. Cell Biol.* 109:971–982.
3. Benavente, R., M. Dabauvalle, U. Scheer, and N. Chaly. 1989. Functional role of newly formed pore complexes in postmitotic nuclear reorganization. *Chromosoma (Berl.).* 98:233–241.
4. Dworetzky, S. I., R. E. Lanford, and C. M. Feldherr. 1988. The effects of variations in the number and sequence of targeting signals on nuclear uptake. *J. Cell Biol.* 107:1279–1287.
5. Feldherr, C. M. 1965. The effect of the electron-opaque pore material on exchanges through the nuclear annuli. *J. Cell Biol.* 25:43–53.
6. Feldherr, C. M. 1966. Nucleocytoplasmic exchanges during cell division. *J. Cell Biol.* 31:199–203.
7. Feldherr, C. M. 1968. Nucleocytoplasmic exchanges during early interphase. *J. Cell Biol.* 39:49–54.
8. Feldherr, C. M., E. Kallenbach, and N. Schultz. 1984. Movement of a karyophilic protein through the nuclear pores of oocytes. *J. Cell Biol.* 99:2216–2222.
9. Frens, G. 1973. Controlled nucleation for the regulation of the particle size in monodisperse gold suspensions. *Nature (Lond.).* 241:20–22.
10. Frost, S. C., and M. D. Lane. 1985. Evidence for the involvement of vicinal sulfhydryl groups in insulin-activated hexose transport by 3T3-L1 adipocytes. *J. Biol. Chem.* 260:2646–2652.
11. Graessmann, A., M. Graessmann, and C. Mueller. 1980. Microinjection of early SV40 DNA fragments and T antigen. *Methods Enzymol.* 65: 816–825.
12. Ingber, D. E., and J. Folkman. 1989. Tension and compression as basic determinants of cell form and function: utilization of a cellular tensegrity mechanism. *In* Cell Shape: Determinants, Regulation, and Regulatory Role, W. D. Stein and F. Bronner, editors. Academic Press, New York. 3–31.
13. Ingber, D. E., J. A. Madri, and J. Folkman. 1987. Endothelial growth factors and extracellular matrix regulate DNA synthesis through modulation of cell and nuclear expansion. *In Vitro Cell. & Dev. Biol.* 23:387–394.
14. Jiang, L., and M. Schindler. 1988. Nuclear transport in 3T3 fibroblasts: effects of growth factors, transformation and cell shape. *J. Cell Biol.* 106:13–19.
15. Kingsley, R. E., and N. L. Cole. 1988. Preparation of cultured mammalian cells for transmission and scanning electron microscopy using Aclar film. *J. Electron Microsc. Tech.* 10:77–85.
16. Lanford, R. E., R. G. White, R. G. Dunham, and P. Kanda. 1988. Effect of basic and nonbasic amino acid substitutions on transport induced by simian virus 40 T-antigen synthetic peptide nuclear transport signals. *Mol. Cell. Biol.* 8:2722–2729.
17. Levine, E. M., Y. Becker, C. W. Boone, and H. Eagle. 1965. Contact inhibition, macromolecular synthesis and polyribosomes in cultured human diploid fibroblasts. *Proc. Natl. Acad. Sci. USA.* 53:350–356.
18. Masurovsky, E. B., E. R. Peterson, and S. M. Crain. 1971. ACLAR film reticles for precise cell localization in nerve tissue cultures. *In Vitro.* 6S:379.
19. Maul, G. G. 1977. The nuclear and cytoplasmic pore complex: structure, dynamics, distribution and evolution. *Int. Rev. Cytol. (Suppl.).* 6:75–186.
20. Maul, G. G., H. M. Maul, J. E. Scogna, M. W. Lieberman, G. S. Stein, B. Y. Hsu, and T. W. Borun. 1972. Time sequence of nuclear pore formation in phytohemagglutinin-stimulated lymphocytes and in HeLa cells during the cell cycle. *J. Cell Biol.* 55:433–447.
21. Newmeyer, D. D., and D. J. Forbes. 1988. Nuclear import can be separated into distinct steps *in vitro*: nuclear pore binding and translocation. *Cell.* 52:641–653.
22. Paine, P. L., L. C. Moore, and S. B. Horowitz. 1975. Nuclear envelope permeability. *Nature (Lond.).* 254:109–114.
23. Peters, R. 1986. Fluorescence microphotolysis to measure nucleocytoplasmic transport and intracellular mobility. *Biochim. Biophys. Acta.* 864: 305–359.
24. Richardson, W. D., A. D. Mills, S. M. Dilworth, R. A. Laskey, and C. Dingwall. 1988. Nuclear protein migration involves two steps: rapid binding at the nuclear envelope followed by slower translocation through nuclear pores. *Cell.* 50:465–475.
25. Robbins, E., and N. K. Gonatas. 1964. The ultrastructure of a mammalian cell during the mitotic cycle. *J. Cell Biol.* 21:429–463.
26. Spurr, A. R. 1969. A low viscosity resin embedding medium for electron microscopy. *J. Ultrastruct. Res.* 26:31–43.
27. Swanson, J. A., and P. L. McNeil. 1987. Nuclear reassembly excludes large macromolecules. *Science (Wash. DC).* 238:548–550.